



Comparison of SEM and optical analyses of DT neutron tracks in CR-39 detectors

P.A. Mosier-Boss^{a,*}, L.P.G. Forsley^b, P. Carbonnelle^c, M.S. Morey^d, J.R. Tinsley^d, J.P. Hurley^d, F.E. Gordon^a

^a SPAWAR Systems Center Pacific, Code 71730, San Diego, CA 92152, USA

^b JWK International Corp., Annandale, VA 22003, USA

^c Université catholique de Louvain, B-1348 Louvain-la-Neuve, Belgium

^d National Security Technologies, LLC, Special Technologies Laboratory, Santa Barbara, CA 93111, USA

ARTICLE INFO

Article history:

Received 8 March 2011

Received in revised form

29 August 2011

Accepted 5 October 2011

Keywords:

CR-39

Neutrons

Microscopy

ABSTRACT

A solid state nuclear track detector, CR-39, was exposed to DT neutrons. After etching, the resultant tracks were analyzed using both an optical microscope and a scanning electron microscope (SEM). In this communication, both methods of analyzing DT neutron tracks are discussed.

Published by Elsevier Ltd.

1. Introduction

Columbia Resin 39, CR-39, is a polyallyldiglycol carbonate polymer. The most common use of this optically clear, amorphous, thermoset plastic is in the manufacture of optical lenses. However, Cartwright et al. (1978) were the first to demonstrate that CR-39 could be used as a solid state nuclear track detector (SSNTD) to detect energetic nuclear particles. As an energetic, charged particle traverses through CR-39, it creates along its path an ionization trail that is more sensitive to chemical etching than the bulk material (Cartwright et al., 1978; Bhakta et al., 1999). After etching, the tracks due to energetic particles have the appearance of holes or pits. The most common method employed to analyze these tracks is optical microscopy. However, atomic force microscopy (AFM) (Yasuda et al., 1999; Palmino et al., 1999; Zhai et al., 2003; Yamauchi et al., 2003) and scanning electron microscopy (SEM) (Fromm et al., 1996; Sartowska et al., 2005; Rana et al., 2007; Lounnis-Mokrani et al., 2008; Abdel-Rahman et al., 2006; Szydlowski et al., 2005; Oganessian et al., 2005) have also been used to analyze tracks in CR-39. In these earlier communications, SEM/AFM analysis was done on tracks resulting from exposure to either alpha or proton sources. In this communication, tracks resulting from exposure to a DT neutron source were examined both optically and by SEM. The purpose of the analysis was to compare the two techniques and to

determine whether additional information on track geometry could be obtained by SEM analysis.

2. Experimental

2.1. Preparation of DT neutron tracks in CR-39 detectors

CR-39 detectors (Fukuvi) were exposed to DT neutrons generated by a Thermo Fisher model A290 neutron generator. The neutron generator has a particle accelerator, i.e., neutron tube. Neutron tubes have several components including an ion source, ion optic elements, and a beam target; all of these are enclosed within a vacuum tight enclosure. The beam target is titanium loaded with tritium. The ion source creates deuteron ions that are extracted by an electric field into the accelerator region, and accelerated toward the target. The detectors were exposed to neutrons at a rate of 10^7 neutrons s^{-1} for 4.5 h. Afterwards, the CR-39 detectors were etched in an aqueous 6.5 N sodium hydroxide solution at 65 °C for 6 h. After etching, the detectors were rinsed in water, vinegar, and again in water. After drying, the detectors were subjected to analysis using both an optical microscope and an SEM.

2.2. Analysis of CR-39 detectors

Optical microscopic examination of the etched CR-39 detectors was done using an Eclipse E600 epifluorescent microscope (Nikon) equipped with a CoolSnap HQ CCD camera (Photometrics). A magnification of 1000× was used. The software used to obtain the

* Corresponding author. Tel.: +1 619 553 1603.

E-mail address: pam.boss@navy.mil (P.A. Mosier-Boss).

images was MetaVue (MDS Analytical Technologies). SEM images were obtained using the LEO 982 Field Emission scanning electron microscope (FE-SEM, Carl Zeiss SMT Inc) that has a secondary scattered electron in-lens detector. For unmetallized samples, an accelerated voltage of 1 keV was used to obtain the images. CR-39 detectors are non-conductive. Operating the electron beam at a lower voltage reduces charging of the non-conductive surface (Joy and Joy, 1996).

2.3. Modeling of alpha tracks comprising the triple track

Nikezic and Yu (2003, 2006) developed TRACK_TEST, a computer program that is used to model alpha tracks incident on CR-39 detectors. In this communication, TRACK_TEST was used to computer model the alpha tracks that comprise the triple tracks. While alpha particles leave tracks on the surface of the CR-39 detector, the neutron reaction, that causes the carbon atom to shatter to form the triple track, can occur anywhere inside the detector. Consequently, TRACK_TEST can only be used to model triple tracks that occurred near the surface of the detector.

The TRACK_TEST program calculates track parameters, such as the lengths of the major and minor axes and the track depth. The computer program also plots the profile for the etch pit in the SSNTD. The executable program is freeware and can be downloaded from the City University of Hong Kong Trackology Research website. When using TRACK_TEST, the input parameters are particle energy, incident angle, etch rate, and etch time. The track etch rate function used to model the Fukuvi CR-39 detectors used in these experiments is (Brun et al., 1999)

$$V_T = V_B \left(e^{(-a_1 x + a_4)} - e^{(-a_2 x + a_3)} + e^{a_3} - e^{a_4} + 1 \right) \quad (1)$$

where V_T and V_B refer to the rates of etching the track and the bulk respectively and x is the residual range of the alpha particle. The optimum values of the coefficients, that describe alpha tracks in Fukuvi CR-39, are $a_1 = 0.1$, $a_2 = 1$, $a_3 = 1.27$, and $a_4 = 1$.

3. Results and discussion

3.1. Neutron interactions with CR-39

Besides charged particles, CR-39 can be used to detect neutrons. These detectors have been used extensively in the inertial-confinement-fusion (ICF) field to determine neutron yields from DD and DT implosion reactions (Frenje et al., 2002; Séguin et al., 2003). In order to detect neutrons with CR-39, the neutron must either scatter or undergo a nuclear reaction with the atomic constituents that make up the detector. These reactions create a moving, charged particle inside the detector. It is the track of this neutron generated charged particle that is revealed upon etching. Fig. 1a shows tracks in CR-39 observed, using an optical microscope at 1000 \times magnification, in a CR-39 detector that has been exposed to a DT neutron source. As will be discussed below, the size and shape of the tracks can be used to determine the type of neutron interaction that created it.

The possible DD (2.45 MeV) and DT (14.1 MeV) neutron interactions with CR-39 are described in Fig. 2a (Frenje et al., 2002). In the interaction shown in case 1, the DD and DT neutrons can scatter elastically. This interaction produces recoil protons, carbons and/or oxygen nuclei in the forward direction. The DT neutrons can also undergo inelastic reactions (n,p) and (n,α) reactions with carbon and oxygen nuclei, case 2 and case 3, respectively in Fig. 2a. These two inelastic reactions result in charged particles that can produce tracks on both the front and back sides of the CR-39 detector. These knock-on tracks resulting from these interactions will appear uniformly throughout the CR-39 detector. In Fig. 1a, track 2 is very small. Such small tracks are latent tracks resulting from knock-on reactions that have occurred deeper in the plastic. Additional etching to remove the plastic will reveal these tracks.

Case 3 interaction schematically shown in Fig. 2a includes both the (n,α) reaction (solid arrows) and the carbon break-up reaction (dotted arrows) (Frenje et al., 2002). The main constituent of CR-39, by weight, is carbon-12, which can be used as both a target and

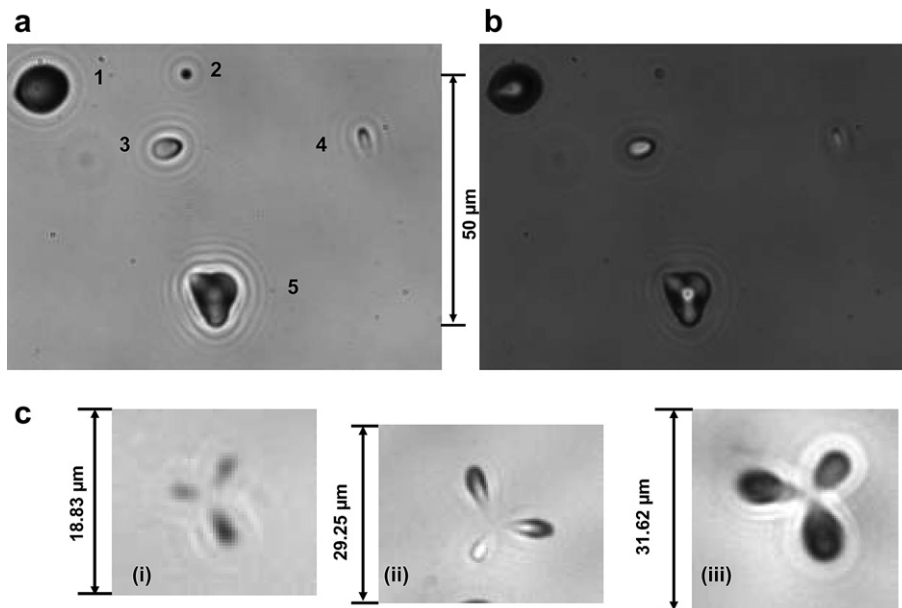


Fig. 1. Optical images of representative DT neutron tracks. (a) Optical microscope image of pits in CR-39 created by exposure to a DT neutron source. Magnification is 1000 \times . (b) Optical image of the area indicated in (a) obtained at a magnification of 1000 \times . The top image was obtained by focusing the microscope optics on the surface of the detector. The bottom image is an overlay of two images taken at two different focal lengths (surface and bottom of the pits). (c) Photomicrographs of triple tracks observed in the same CR-39 detector resulting from carbon break-up reactions occurring at different depths inside the plastic.

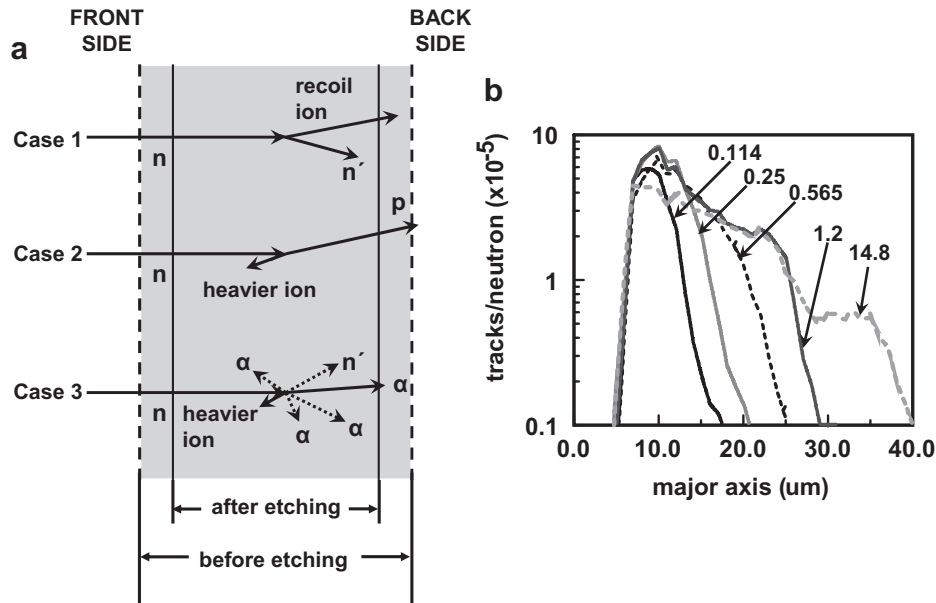
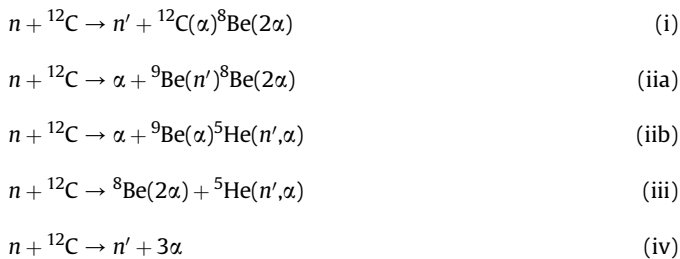


Fig. 2. Summary of neutron interactions with CR-39 and how the size of the tracks is used to identify the neutron interaction with the detector. (a) Diagram illustrating the three neutron interactions that can take place inside a CR-39 detector (Frenje et al., 2002). The drawing is not to scale. DD neutrons undergo the interaction shown in case 1 while DT neutrons undergo all three types of interactions. (b) Track size distribution for CR-39 detectors that have been exposed to neutrons (Abdel-Moneim and Abdel-Naby, 2003). The energies of the neutrons, in MeV, are indicated.

a detector for energetic neutrons (Antolković and Dolenc, 1975). The carbon break-up reaction in CR-39 is the one neutron interaction that is easily identified. In the carbon break-up reaction, a metastable ^{13}C is formed that then shatters into two or three alpha particles. The residuals of the reaction can be viewed in the CR-39 detector as a symmetric or asymmetric triple track (Abdel-Moneim and Abdel-Naby, 2003). In the triple track, each prong represents the alpha particle that occurs in the decay. In Fig. 1a, track 5 is an example of a triple track. With the microscope optics focused on the surface of the detector, it can be seen that the track has three lobes. Fig. 1b is an overlay image of two microphotographs obtained at two focusing depths, the surface and the bottom of the pits. In this image, it can be seen that the three lobes are breaking away from a center point. These features are diagnostic of a triple track.

The triple tracks in Fig. 1c are different in shape from that shown in Fig. 1a. The neutron reaction that can cause a carbon to shatter can proceed to the four-body final state through one or more of the following reaction mechanisms (Antolković and Dolenc, 1975):



Processes (i)–(iii) are sequential decays going through different excited states of intermediate systems and process (iv) is a simultaneous four-body break-up. It is believed that these different pathways will result in triple tracks with different shapes. Additional work needs to be done to match these shapes with the appropriate pathway. This is not the scope of the current communication.

Like the proton/carbon/oxygen recoils, the carbon break-up reaction can occur anywhere throughout the CR-39 detector. This is illustrated in Fig. 1c that shows triple tracks observed on one CR-39 detector. In Fig. 1c(i), three faint tracks are observed. The center point, where the three tracks break away from, is not apparent. In Fig. 1c(ii), the lobes making up the triple track are better defined. However, the center point is still not observed indicating that it is deeper inside the plastic. In Fig. 1c(iii), the lobes of the triple track are larger than those observed for either triple track shown in Fig. 1c(i) or (ii). However, the three lobes do not quite meet in the center, indicating that the center point is just below the surface. Therefore, the carbon break-up reaction that resulted in the triple track in Fig. 1c(iii) occurred near the surface of the detector, resulting in larger tracks. The carbon break-up reactions that created the triple tracks shown in Fig. 1c(i) and (ii) occurred deeper inside the detector with Fig. 1c(i) occurring the deepest inside the plastic.

Phillips et al. (2006) showed that the track sizes can be used to differentiate recoil protons and recoil carbons/oxygens. Fig. 2b shows the track size distributions obtained for neutrons whose energies range from 0.144 to 14.8 MeV. At low neutron energies, only recoil protons are seen and are observed as a peak at $\sim 10 \mu\text{m}$ (0.144 MeV neutron in Fig. 2b). As the neutron energy increases, a broadening of the proton recoil peak at $\sim 10 \mu\text{m}$ is observed. At a neutron energy of 1.2 MeV, a second peak is visible at $\sim 25 \mu\text{m}$, Fig. 2b. This second peak is attributed to recoil carbon and oxygen atoms. For neutron energies between 1.2 and 8 MeV, the size distribution of tracks observed in the CR-39 detectors is roughly similar. In the CR-39 detector exposed to 14.8 MeV neutrons, a peak is observed at $\sim 35 \mu\text{m}$. This peak is attributed to the three alpha particle reaction.

The tracks shown in Fig. 1a and b are representative of the tracks resulting from the three kinds of neutron interactions with the constituents of CR-39. The sizes and shapes of these tracks can be used to identify the neutron reaction that created them. In Fig. 1a and b, track 5 has already been identified as a triple track. The small tracks 3 and 4 are attributed to proton recoils while the large track 1 is either a carbon or oxygen recoil.

3.2. Optical and SEM analyses of DT neutron tracks

In order to obtain the optical images of the tracks shown in Fig. 1, the CR-39 detectors are backlit. Consequently, the appearance of the observed image depends upon the manner in which the track has scattered and reflected the light passing through it. The Trackology Research Group of Nikezic and Yu has done a thorough analysis of light scattering of alpha tracks in SSNTDs such as CR-39 and PADC and the resultant effects of the light scattering on the observed optical image (Nikezic and Yu, 2004, 2008; Nikezic et al., 2005; Yu et al., 2007). From their studies, they discovered that the major factors affecting the track appearance were the total internal reflection and inclination angles of elements in a track wall with respect to the light rays. Their analysis has shown that dark areas in the images indicate that total internal reflection of light has occurred. This is indicative of either steep track walls or a perfectly conical track. Bright areas inside a track indicate that light rays coming from below the track are refracted through very small angles in the central area. As a result, the intensity loss is relatively small causing the central area to be very bright. Bright features inside a track are indicative of spherical or rounded bottoms. In CR-39, spherical/rounded bottoms result when etching has occurred past the endpoint of the ionization trail created by the particle as it traveled inside the plastic material. In contrast, perfectly conical tracks have steep track walls and the light rays at all points on the track wall will experience total internal reflection. The light rays will also undergo internal reflection on the detector surface. Under these conditions, a perfectly conical track will be completely dark, when viewed top to bottom, using a backlit optical microscope. In SEM, the sample surface is scanned with a beam of electrons in a raster scan pattern. The electrons interact with the atoms that make up the sample producing signals that contain information about the sample's surface topography. In what follows, triple tracks and oxygen/carbon recoil tracks are analyzed using both optical microscopy and SEM.

3.2.1. Asymmetric triple track and carbon/oxygen recoil track

Fig. 3a(i) shows optical images of DT neutron generated tracks obtained at 1000 \times magnification and with the microscope optics focused on the surface of the detector. At this magnification,

diffraction rings are observed around the tracks indicating that the microscope is operating close to its diffraction limit, which, in turn, determines the resolution of the microscope. For optical microscopes, the lowest resolution possible is on the order of 200 nm. Higher resolution is possible using an electron microscope. Fig. 3b shows an SEM of the same tracks as seen in Fig. 3a(i) obtained at a magnification of 3000 \times . No diffraction rings are observed. Fig. 3c shows optical images taken of the tracks after the detector had been subjected to SEM analysis. Even though the electron beam of the SEM was operated at 1 keV, a comparison of the tracks in Fig. 3a and c shows that the electron irradiation did damage the tracks. It also indicates that all optical analysis of the plastic detectors needs to be completed prior to SEM analysis.

Besides being able to obtain higher resolution images, another advantage of SEM images over optical images is that SEM images have a three-dimensional appearance. Optical images are inherently two-dimensional. However, in these investigations, optical images of the tracks were taken with the microscope optics focused on both the surface of the CR-39 detector and at the bottom of the tracks. By overlaying these images, it is possible to make some conclusions about the three-dimensional shape of the track. In Fig. 3a(i), the image was taken with the optical microscope optics focused on the surface of the detector. The observed tracks are dark in color. The track on the left is an asymmetric triple track while the circular track on the right is due to either a carbon/oxygen recoil reaction with a neutron. Fig. 3a(ii) is an overlay of two optical images taken at different focusing depths, namely the surface and the bottom of the pits. Based upon the analysis of Nikezic and Yu (2008), the large bright disk-shaped area inside the circular track suggests that the track has a round bottom and that the track is shallow. This is confirmed by the SEM image of the same track shown in Fig. 3b. No deep indentation is observed showing that the track does not have a conical shape.

The optical image of the triple track in Fig. 3a(i) shows two prongs and is an example of an asymmetric track. The overlay image, Fig. 3a(ii), shows a bright spot in the center (indicated by an arrow). This bright spot, or center point, indicates the impact area where the DT neutron collided with the carbon atom causing it to shatter. The bright streaks emanating from the center point indicate the direction the resultant alpha particles moved from the

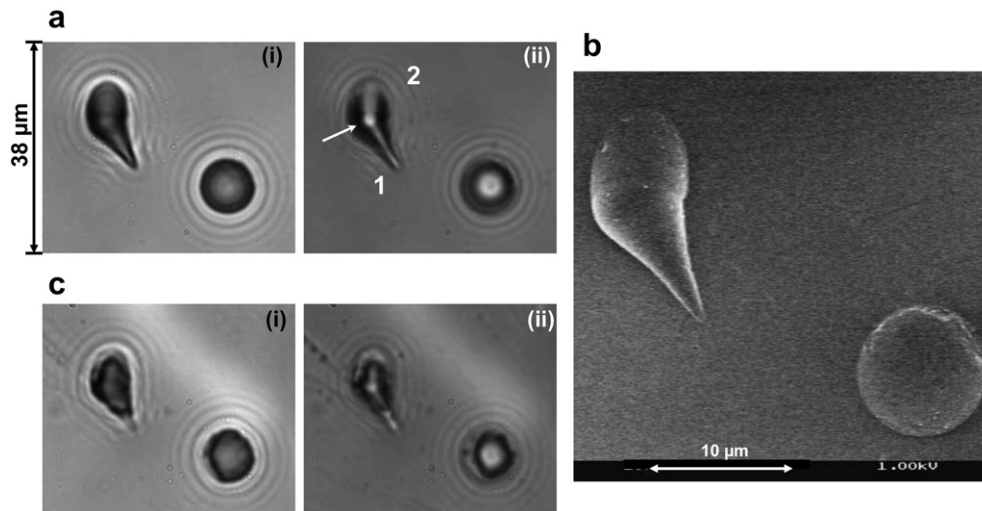


Fig. 3. SEM and optical images, taken before and after SEM analysis, of DT neutron tracks. (a) Optical image of DT tracks taken at 1000 \times magnification. This image was taken before the detector was subjected to SEM analysis. Arrow indicates the break-away point for the alpha particles created when the neutron impacted the carbon atom causing it to shatter. (b) SEM image of the same DT tracks as in (a) taken at 3000 \times magnification. (c) Optical image of DT tracks taken at 1000 \times magnification. This image was taken after the detector was subjected to SEM analysis. In both (a) and (c), (i) was obtained by focusing the microscope optics on the surface of the detector while (ii) is an overlay of two images taken at two different focal lengths (surface and bottom of the pits).

Table 1

Measured and calculated track diameters for the alpha tracks comprising the triple track shown in Fig. 3a. Etch time is 6 h and etch rate is $1.25 \mu\text{m h}^{-1}$. The tracks are indicated in Fig. 3a.

Alpha track	Measured values		Calculated values				
	Major axis (μm)	Minor axis (μm)	Energy (MeV)	Incident angle ($^\circ$)	Major axis (μm)	Minor axis (μm)	Depth (μm)
1	13.12 ± 0.48	6.21 ± 0.48	2.45	27	13.03	6.58	1.47
2	11.05 ± 0.48	7.60 ± 0.48	1.8	30	10.75	7.35	1.43

center point. The brightness indicates that the bottoms of the tracks are rounded and that etching has gone past the endpoint of the particle in the detector material. The SEM image of this track, Fig. 3b, shows that the tracks do not have a conical shape and that the bottoms are rounded. It is unlikely that the third prong of the asymmetric track occurred above the etched surface of the detector. If this were the case, the track resulting from this hypothetical alpha would begin etching first. As the etching continues, this track would have gotten bigger and shallower (Al-Najjar et al., 1986) and some residual of it would have been apparent in both the optical and SEM images, Fig. 3a and b. This is not observed. An asymmetric triple track may result when the third prong is below the etch pit. If this were the case, the third prong may not be visible in the optical image. Alternatively, asymmetric triple tracks could result from energetics. One of the three alpha particles may not have sufficient energy to make an etchable track and, as a result, cannot be observed (Aframian, 1983). The SEM image of the track, Fig. 3b, shows no opening for a third prong indicating that the third alpha particle did not have enough energy to create an etchable track.

In order to model the alpha tracks comprising a triple track, the major and minor axes of each alpha track need to be measured. How this is done for the triple track shown in Fig. 3a is described in

the supplementary material. The alpha tracks comprising the triple track are numbered in Fig. 3a(ii). Table 1 summarizes the measured major and minor axes for each track. Track modeling of the alpha particles was done using TRACK_TEST (Nikezic and Yu, 2003, 2006). The results of the modeling are also summarized in Table 1. The modeling indicates that the depths of the two alpha tracks are approximately the same. The SEM image of the triple track, Fig. 3b, also shows that the depths of both alpha tracks making up the triple track are about the same. The bright features in the optical images and the shallowness of the tracks indicate that etching has gone past the endpoints of the ionization trails of the alpha particles. Because etching has gone past the endpoints, it is not possible to make any additional conclusions as to the geometry of the track inside the detector prior to etching.

3.2.2. Symmetric triple track and carbon/oxygen recoil tracks

Fig. 4a(i) shows an optical image of three DT neutron generated tracks obtained at $1000\times$ magnification and with the optics focused on the surface of the detector. Fig. 4a(ii) is an overlay of two images taken on the surface of the detector and at the bottom of the pits. The middle track is circular in shape. The bright spot inside the track is in the center indicating that the recoil ion moved in a direction perpendicular to the surface. The bright spot is better defined than the bright spot shown in the circular track in Fig. 3a(ii). This suggests that the circular track in Fig. 4a(i) is not as shallow as the one in Fig. 3a(ii). The SEM image in Fig. 4b shows that this circular track is deeper than the one shown in Fig. 3b. The top track in Fig. 4a(i) has an elliptical shape. The shape indicates that the recoil particle entered the detector at an oblique angle. A bright, diffuse streak is observed inside the track, Fig. 4a(ii). This indicates that this part of the track will have a curved surface. The SEM image of this track, Fig. 4c, shows that the track is shallow with a dimple on the left-hand side. This dimple could either indicate the

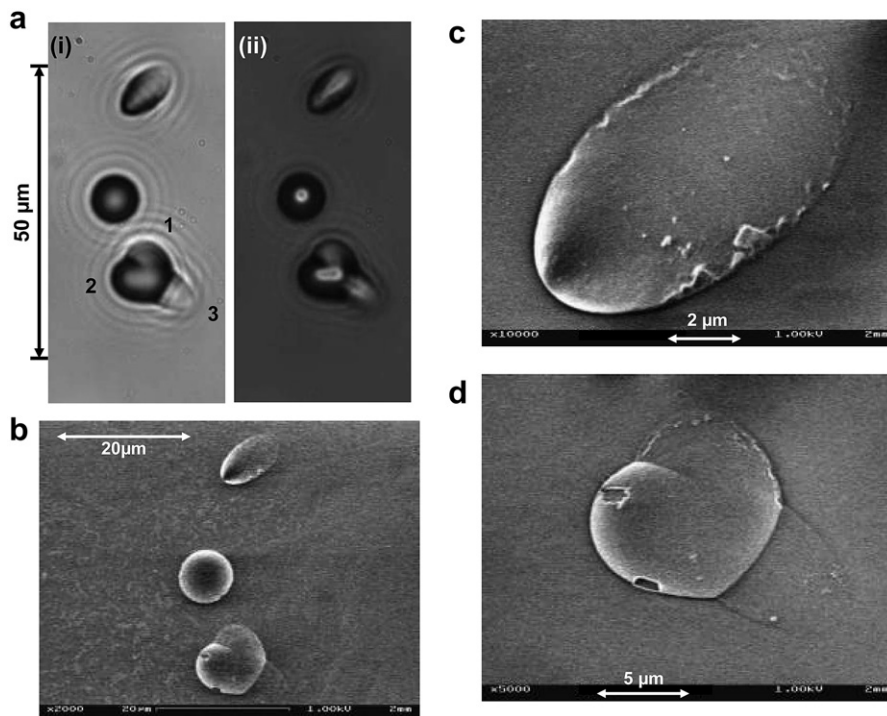


Fig. 4. Optical and SEM analyses of a DT neutron generated symmetric triple track and carbon/oxygen recoil tracks. (a) Optical images of DT tracks taken at $1000\times$ magnification, where (i) was obtained by focusing the microscope optics on the surface of the detector and (ii) is an overlay of two images taken at two different focal lengths (surface and bottom of the pits). (b) SEM image of the same DT tracks shown in (a) obtained at $2000\times$ magnification. (c) SEM image of the top elliptical track in (b) obtained at $10,000\times$ magnification. (d) SEM image of the triple track in (b) obtained at $5000\times$ magnification.

Table 2

Measured and calculated track diameters for the alpha tracks comprising the triple track shown in Fig. 4b. Etch time is 6 h and etch rate is $1.25 \mu\text{m h}^{-1}$. The tracks are indicated in Fig. 4b.

Alpha track	Measured values		Calculated values				
	Major axis (μm)	Minor axis (μm)	Energy (MeV)	Incident angle ($^\circ$)	Major axis (μm)	Minor axis (μm)	Depth (μm)
1	8.06 ± 0.48	6.87 ± 0.48	1.0	35	8.10	7.01	1.06
2	8.29 ± 0.48	7.10 ± 0.48	1.1	35	8.51	7.25	1.17
3	10.43 ± 0.48	5.69 ± 0.48	2.0	23	10.39	6.02	0.723

endpoint of the recoil particle that entered the detector or the start point of a particle due to a recoil occurring inside the detector below the etch plane.

The bottom track in Fig. 4a(i) is a symmetric triple track. Fig. 4a(ii), an overlay of two images taken at the surface and the bottom of the pits, shows tracks from the three alphas breaking away from a center point. In Fig. 4a(i), lobes 1 and 2 are darker than lobe 3 suggesting that track 3 is shallower than tracks 1 and 2. The SEM image of the triple track, Fig. 4d, shows that this is indeed the case.

Track modeling of the alpha particles was done using TRACK_TEST (Nikezic and Yu, 2003, 2006). The results are summarized in Table 2. The modeling indicates that, while all three tracks are shallow, track 3 is shallower than tracks 1 and 2. As discussed *vide supra*, the bright features in the optical images and the shallowness of the tracks, as seen in the SEM image, indicate that etching has gone past the endpoints of the ionization trails of the alpha particles. Knowing the energies of the alpha particles

comprising the triple track, the energy of the neutron that created the triple track can be estimated using the following relationship:

$$E_n = E_{th} + E_{\alpha 1} + E_{\alpha 2} + E_{\alpha 3} \quad (2)$$

where E_n and E_{th} are the energy of the neutron that created the triple track and the threshold energy required to shatter a carbon atom, respectively, and $E_{\alpha 1}$, $E_{\alpha 2}$, and $E_{\alpha 3}$ are the energies of the alpha particles formed. The threshold energy of a neutron required to shatter a carbon atom is 9.6 MeV (Aframian, 1983). The energies of the alpha particles are tabulated in Table 2. Using equation (2), the energy of the neutron that created the triple track shown in Fig. 4b is estimated to be 13.7 MeV, which is consistent with the expected value for a DT neutron source (11.9–17.5 MeV) (Séguin et al., 2003).

3.2.3. Geometrical analysis of shallow symmetric triple tracks

Fig. 5a and b is optical photomicrographs of the same triple track shown in Fig. 1c(iii). The magnification to obtain these images was $1000\times$. Fig. 5a is obtained by focusing the microscope optics on the surface of the detector while Fig. 5b is an overlay of two images taken at two different focal lengths – the surface of the detector and the bottom of the tracks. Fig. 5c is an SEM image of this track obtained at $5000\times$ magnification. The bright areas shown in Fig. 5b indicate that the bottom of each track is rounded. This is verified by the SEM image in Fig. 5c. Both the optical and SEM images indicate that the center point, from which the three alpha particles break away, is below the surface of the etched detector. Fig. 5d shows the SEM of the triple track with the three alpha tracks drawn in. Dashed lines indicate features that are below the surface of the etched detector. The ovals indicate the openings of the tracks. The outlines of these openings are barely observable in the SEM image of the

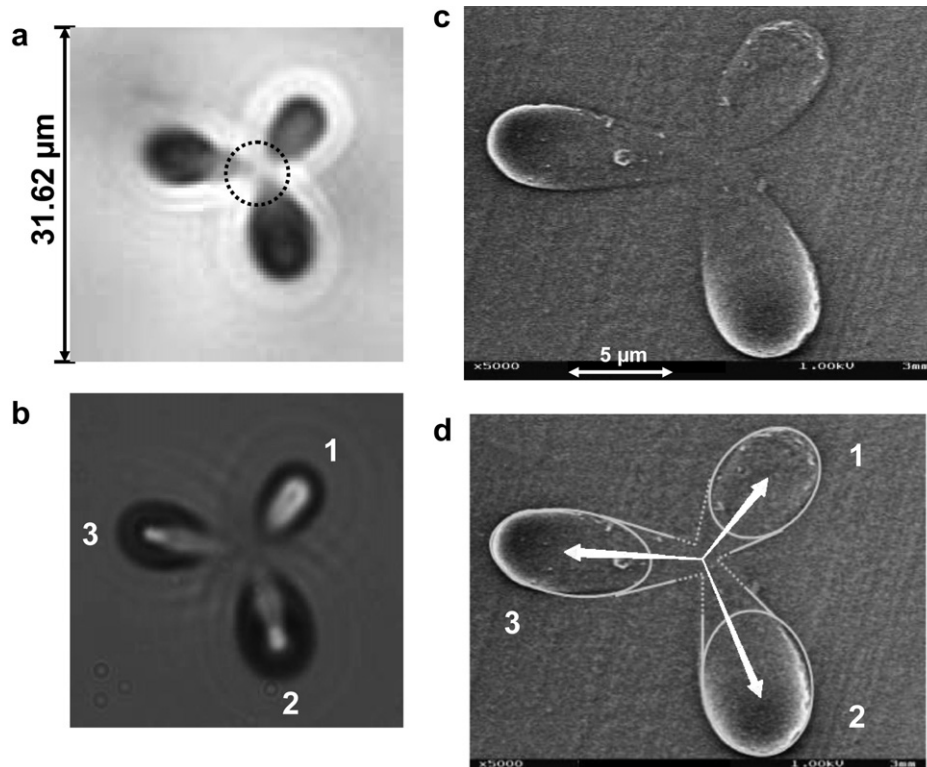


Fig. 5. Optical and SEM analyses of a DT neutron generated symmetric triple track whose center point is beneath the plastic. (a) Optical image of the same DT triple track shown in Fig. 1c(i). The image was taken at $1000\times$ magnification and by focusing the microscope optics on the surface of the detector. The circled area indicates where the three alpha tracks break away from a center point. (b) Optical image of the triple track shown in (a) obtained by overlaying two images taken at two different focal lengths (surface and bottom of the pits). The lobes of the triple track are numbered. (c) SEM image of the same DT tracks as (a) obtained at $5000\times$ magnification. (d) SEM of the triple track with the alpha tracks drawn in and numbered. Dashed lines indicate the portions of the track are under the etched surface of the detector. The trajectories of the alpha particles are indicated.

Table 3

Measured and calculated track diameters for the alpha tracks comprising the triple track shown in Fig. 5. Etch time is 6 h and etch rate is $1.25 \mu\text{m h}^{-1}$. The tracks are indicated in Fig. 5b.

Alpha track	Measured values		Calculated values				
	Major axis (μm)	Minor axis (μm)	Energy (MeV)	Incident angle ($^\circ$)	Major axis (μm)	Minor axis (μm)	Depth (μm)
1	8.57 ± 0.48	5.14 ± 0.48	1.5	24	8.49	5.38	0.65
2	10.93 ± 0.48	6.68 ± 0.48	2.0	27	11.16	6.68	1.22
3	11.25 ± 0.48	5.57 ± 0.48	2.2	24	11.47	5.70	0.92

alpha tracks making up the triple track, Fig. 5c. This indicates that etching came very close to breaking through the tubes created by the etchant as it etched the ionization trails formed by the alpha particles as they traveled through the plastic. The arrows in Fig. 5d show the trajectories of the alpha particles as they broke away from the center point.

The etching process was terminated before the etchant reached the center point. However in the optical image, Fig. 5a, a faint outline of the center point can be seen. The center point is not obvious in the SEM image, Fig. 5c. These images indicate that the etchant was able to etch out the center point, but that the center point is beneath a thin plastic film. A better example of undercutting a track inside the plastic will be shown *vide infra*.

Track modeling of the alpha particles was done using TRACK_TEST (Nikezic and Yu, 2003, 2006). The results are summarized in Table 3. Knowing the energies of the alpha particles comprising the triple track, the energy of the neutron that created the triple track was estimated, using Eqn. (2), to be 15.3 MeV.

Another example of a symmetric triple track is shown in Fig. 6. Figs. 6a and b are optical images taken at $1000\times$ magnification. To obtain the photomicrograph shown in Fig. 6a, the microscope optics were focused on the surface of the etched detector. Fig. 6b is obtained by overlaying two images obtained at two different focusing depths (surface of the detector and the bottom of the pits). The bright regions seen in Fig. 6b indicate that the bottoms of the tracks are rounded. This is verified by the SEM image of the triple track, Fig. 6c. Unlike the triple track shown in Fig. 5, the center point can be seen in the SEM image shown in Fig. 6c. From the SEM image it can be concluded that the etchant completely etched through the tubes created by the etchant as it, progressively, etched away the bulk CR-39 and the alpha particle-generated ionization trails inside the detector.

In the case of the triple track shown in Fig. 6, the lobes comprising the triple track are approximately the same size. This indicates that the alpha particles have the same energy. The four-body break-up reaction, $n + {}^{12}\text{C} \rightarrow n' + 3\alpha$, would result in three alpha particles of the same energy (Antolković and Dolenc, 1975).

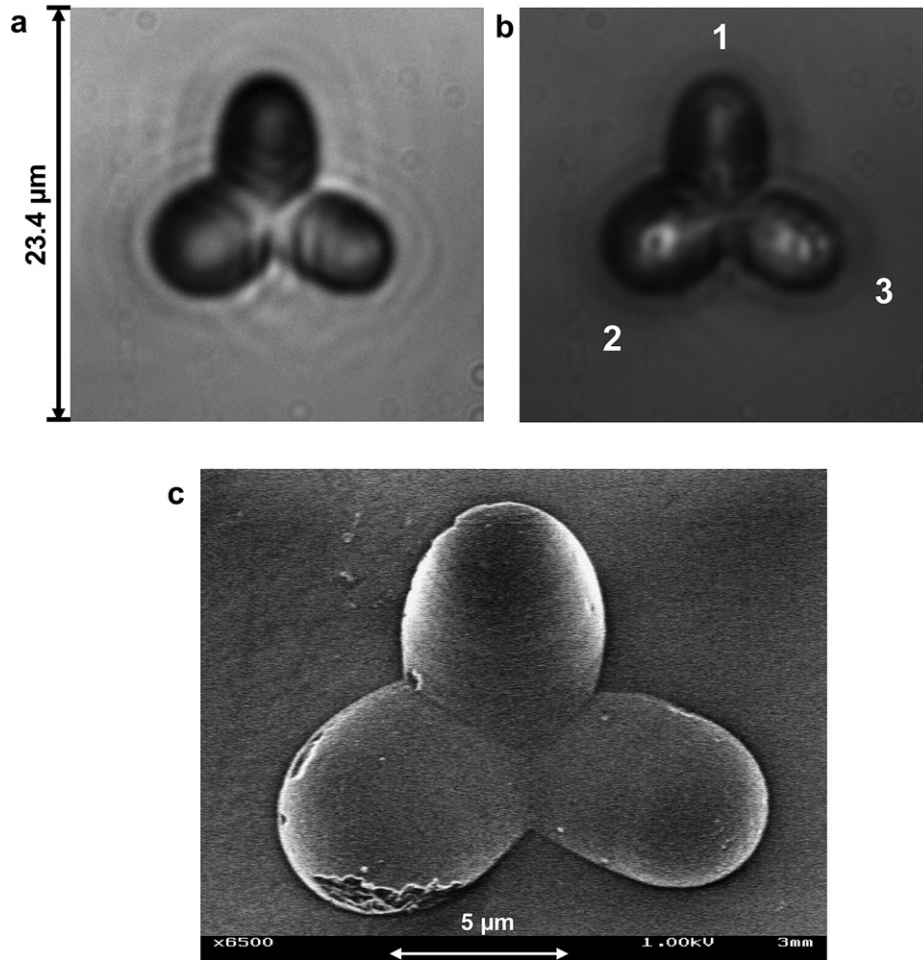


Fig. 6. Optical and SEM analyses of a DT neutron generated symmetric triple track where the etchant has etched through the tubes created by the ionization trails inside the detector. (a) Optical image of a DT triple track taken at $1000\times$ magnification and with the microscope optics focused on the surface of the detector. (b) Optical image of the triple track shown in (a) obtained by overlaying two images taken at two different focal lengths (surface and bottom of the pits). The lobes of the triple track are numbered. (c) SEM image of the same triple track tracks as (a) obtained at $6500\times$ magnification.

Table 4

Measured and calculated track diameters for the alpha tracks comprising the triple track shown in Fig. 6. Etch time is 6 h and etch rate is $1.25 \mu\text{m h}^{-1}$. The tracks are indicated in Fig. 6b.

Alpha track	Measured values		Calculated values				
	Major axis (μm)	Minor axis (μm)	Energy (MeV)	Incident angle ($^\circ$)	Major axis (μm)	Minor axis (μm)	Depth (μm)
1	7.59 ± 0.48	6.80 ± 0.48	1.1	30	7.86	6.31	0.085
2	8.22 ± 0.48	6.01 ± 0.48	1.2	28	7.97	6.06	0.079
3	7.59 ± 0.48	5.69 ± 0.48	1.1	28	7.55	5.85	0.072

Track modeling of the alpha particles was done using TRACK_TEST (Nikezic and Yu, 2003, 2006). The results are summarized in Table 4. Knowing the energies of the alpha particles comprising the triple track, the energy of the neutron that created the triple track was estimated, using Eqn. (2), to be 13.0 MeV.

3.2.4. Geometrical analysis of a deep symmetric triple track

Figs. 7a and b show optical and SEM images, respectively, of DT neutron tracks taken at the same magnification, $1000\times$. The optical image shown in Fig. 7a(i) is taken with the microscope optics focused on the surface of the detector while that shown in Fig. 7a(ii) is an overlay of two images taken at the surface and the bottom of the pits. The right hand track in both Fig. 7a and b has a pear shape indicating that the neutron recoil ion entered the detector at an oblique angle. The left-hand track in Fig. 7a and b is a triple track. The tracks due to the alpha particles making up the triple track are dark in color in both Fig. 7a(i) and (ii). This indicates that the light rays are undergoing almost total internal reflection on the detector surface (Yu et al., 2007). This suggests that the track walls are steep. The SEM image of the triple track, Fig. 7c, at $5000\times$ magnification, reveals more details on the structure of the triple track and shows that the left-hand prong is not continuous and that the right hand prong is actually below the surface of the etched detector. These features were not obvious in the optical images and these images, Fig. 7a and c, show that the two imaging techniques, optical and SEM, are complementary.

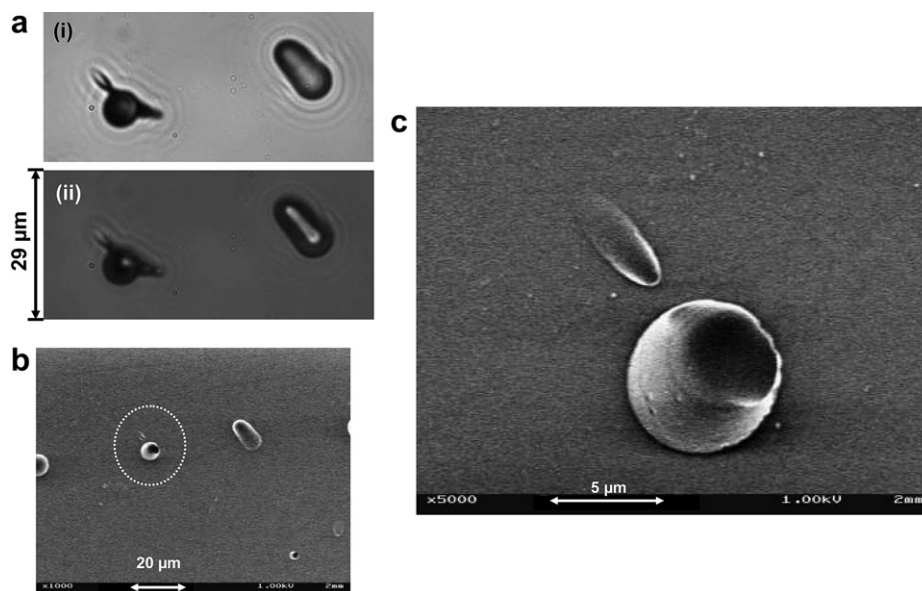


Fig. 7. Optical and SEM images of a DT neutron generated symmetric triple track, created deep inside the detector, and a carbon/oxygen recoil track. (a) Optical images of DT tracks taken at $1000\times$ magnification, where (i) is obtained by focusing the microscope optics on the surface of the detector and (ii) is an overlay of two images taken at two different focal lengths (surface and bottom of the pits). (b) SEM image of the same DT tracks as (a) obtained at $1000\times$ magnification. The triple track is circled. (c) SEM image of the triple track in (b) obtained at $5000\times$ magnification.

Figs. 8a and b are the optical images of just the triple track. In Fig. 8b, the tracks are numbered and the trajectories the alpha particles took inside the plastic are shown. In Fig. 8c, the SEM image of the triple track is shown with the three alpha tracks drawn in. The fact that all of track two and part of track 1 are below the surface of the plastic indicates that the carbon break-up occurred below the etch plane. Fig. 8d shows a side-view schematic describing the geometry of the triple track inside the detector. In analyzing the spatial orientations of the tracks inside the detector, there are three surface layers. These are the initial surface of the detector prior to etching, S_i ; the surface of the detector after etching undamaged (bulk) CR-39, S_e ; and the surface that corresponds to the bottom of the etch pit, S_p . In the diagram shown in Fig. 8d, h is the thickness of the layer removed by etching bulk CR-39 at a rate of V_b . In contrast, L is the depth of the track created by etching, at a rate of V_t , the ionization trail created by the charged particle. In the diagram, C corresponds to the center point of the alpha tracks. The arrows indicate the trajectories of the alpha particles, as they broke away from the center point, after the carbon break-up reaction occurred. The dots at the end of the arrows indicate the endpoints of the alpha particles when they came to rest inside the detector. In Fig. 8d, the light gray area is a two-dimensional representation of the track and the dark gray ellipses correspond to the track openings, as observed on the surface of the etched detector.

As indicated by the diagram in Fig. 8d, the etchant will first encounter the ionization trail of the alpha particle responsible for track 3 as the endpoint of this track is closer to the initial surface, S_i , of the detector. The etchant will etch out track 3 ionization trail faster than the bulk. Consequently, this track will become larger and larger as the etching process progresses along the etch plane. Eventually, the etchant will reach the ionization trail due to track 1. Both tracks will then be etched, however, the opening of track 1 will be smaller than that of track 3. The etchant will preferentially etch the ionization trails of the alpha particles making up the triple track over the bulk CR-39. Once the etchant has reached the center point, C , it will begin to etch out the ionization trail due to track 2. Because $V_t > V_b$, track 2 etches out before the etch plane, designated by

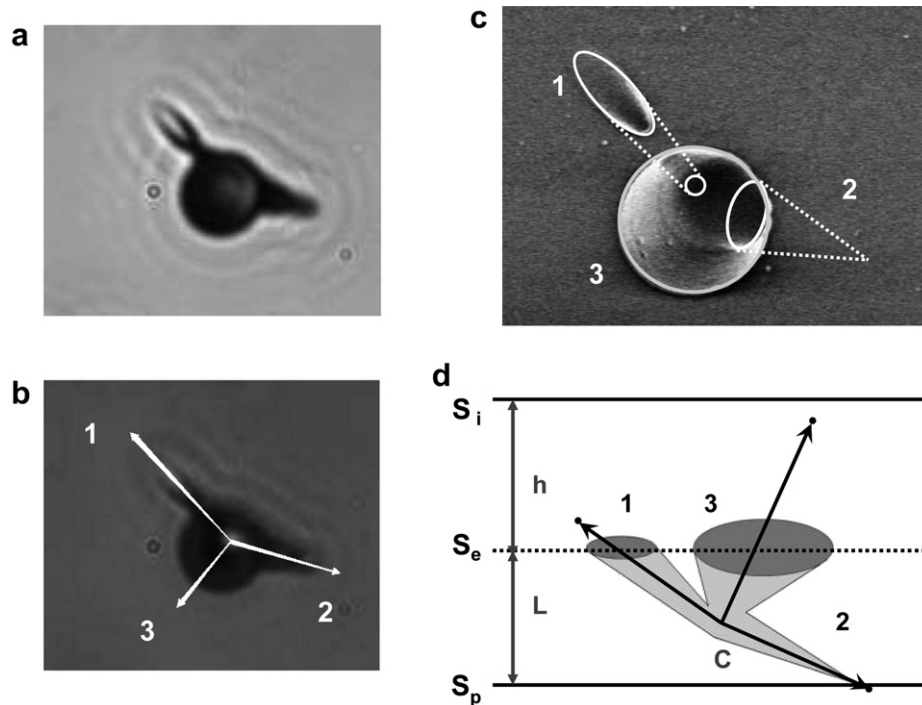


Fig. 8. Analysis of the geometry of a DT neutron generated triple track created inside the CR-39 detector. (a) Optical image of the triple track shown in Fig. 7(a). The image was obtained using a magnification of $1000\times$ and with the microscope optics focused on the surface of the detector. (b) Optical image of the triple track shown in (a) obtained by overlaying two images taken at two different focal lengths (surface and bottom of the pits). The lobes of the triple track are numbered and the trajectories of the alpha particles are indicated. (c) SEM image of the same triple tracks as (a) obtained at $5000\times$ magnification. The alpha tracks are drawn in and numbered. Dashed lines indicate that the track, or portions of the track, are under the etched surface of the detector. (d) Two-dimensional, side-view schematic describing the geometry of the triple track inside the detector. The arrows indicate the trajectory of the alpha particles inside the detector, the dots indicate the endpoints when the alpha particles came to rest, and the gray area indicates the shape of the track. In this schematic, S_i is the initial surface of the detector prior to etching, S_e is the surface of the detector after etching undamaged (bulk) CR-39, S_p is the surface that corresponds to the bottom of the etch pit, h is the thickness of the layer removed by etching bulk CR-39 at a rate of V_b , L is the depth of the track created by etching at a rate of V_t , and C is the center point where the three alpha particles break away to form the triple track.

surface S_e , reaches the track. Track 2 is close enough to the surface S_e that it can be seen in the optical image when the detector is backlit.

4. Conclusions

In this communication, DT neutron generated tracks in CR-39 detectors were analyzed using both an optical microscope and a scanning electron microscope. In this investigation, the highest possible magnification for the optical microscope was $1000\times$. In these images, diffraction rings were observed indicating that the microscope was being operated at its diffraction limit and, consequently, at the highest optical resolution possible. In the optical analysis of the tracks, images were taken at two focusing depths (on the surface of the detector and the bottom of the pits) and were overlaid. Using this method it was possible to make some conclusions as to the geometrical shape of the tracks, i.e. bright areas in the track indicate curvature and dark areas are indicative of steep walls. In contrast, SEM images can be obtained at higher magnifications and the images have a three-dimensional appearance. However, even when the electron beam is operated at a low power, the electron radiation can cause damage to the tracks. Consequently SEM analysis of the tracks should be done after the optical analysis is complete. Back-lighting is used in the optical analysis of the tracks. In contrast, in SEM, the electron beam irradiates the front surface of the detector. The two methods of analysis can be complementary for tracks caused by the ejection of particles below the surface of the etched detector. The SEM analysis shows which tracks are below the surface of the etched detector. If the track is

close to the surface of the detector, the optical images will show the shape of that track. Track modeling can be used to infer the energy of the alpha particles comprising the triple track and, consequently, the energy of the incident neutron that caused the carbon break-up reaction.

Acknowledgments

This effort was funded by the SPAWAR Systems Center Pacific ILIR and S&T Initiatives Programs, the Defense Threat Reduction Agency (DTRA), and JWK Corporation. The authors would also like to thank Dr. Gary Phillips, nuclear physicist, retired from the Naval Research Laboratory, US Navy, Radiation Effects Branch for valuable discussions in interpreting the optical data.

Appendix. Supporting material

Supplementary data associated with this article can be found, in the online version, at doi:10.1016/j.radmeas.2011.10.004.

References

- Abdel-Moneim, A.M., Abdel-Naby, A., 2003. A study of fast neutron beam geometry and energy distribution using triple- α reactions. *Radiat. Meas.* 37, 15–19.
- Abdel-Rahman, M.A., et al., 2006. Effect of alpha-particle energies on CR-39 line-shape parameters using positron annihilation technique. *Prog. Phys.* 3, 66–69.
- Aframian, A., 1983. Disintegration of carbon-12 with 7.1–20.1 MeV neutrons in dielectrics. *J. Phys. G, Nucl. Phys.* 9, 985–994.
- Al-Najjar, S.A.R., et al., 1986. Fast-neutron spectrometry using the triple- α reaction in the CR-39 detector. *Nucl. Tracks* 12, 611–615.
- Antolković, B., Dolenc, Z., 1975. The neutron-induced $^{12}\text{C}(n, n')3\alpha$ reaction at 14.4 MeV in a kinematically complete experiment. *Nucl. Phys. A* 237, 235–252.

- Bhakta, J.R., et al., 1999. Increase in the area of etched alpha-particle tracks in CR-39 plastic with increasing storage time under nitrogen. *Radiat. Meas.* 30, 29–34.
- Brun, C., et al., 1999. Intercomparative study of the detection characteristics of the CR-39 SSNTD for light ions: present status of the Besancon–Dresden approaches. *Radiat. Meas.* 31, 89–98.
- Cartwright, B.G., Shirk, E.K., Price, P.B., 1978. A nuclear-track-recording polymer of unique sensitivity and resolution. *Nucl. Instr. Meth.* 153, 457–460.
- Frenje, J.A., et al., 2002. Absolute measurements of neutron yields from DD and DT implosions at the OMEGA laser facility using CR-39 track detectors. *Rev. Sci. Instrum.* 73, 2597–2605.
- Fromm, M., et al., 1996. Ion track etching in isotropic polymers: etched track shape and detection efficiency. *Nucl. Instr. Meth. B* 107, 337–343.
- <http://www.cityu.edu.hk/ap/nru/test.htm>.
- Joy, D.C., Joy, C.S., 1996. Low voltage scanning electron microscopy. *Micron* 27, 247–263.
- Lounnis-Mokrani, Z., et al., 2008. Determination of the proton latent track dimensions in CR-39 detectors using small angle neutron scattering. *Radiat. Meas.* 43, S41–S47.
- Nikezic, D., Yu, K.N., 2003. Three-dimensional analytical determination of the track parameters: over-etched tracks. *Radiat. Meas.* 37, 39–45.
- Nikezic, D., Yu, K.N., 2004. Formation and growth of tracks in nuclear track materials. *Mater. Sci. Eng. R* 46, 51–123.
- Nikezic, D., Yu, K.N., 2006. Computer program TRACK_TEST for calculating parameters and plotting profiles for etch pits in nuclear track materials. *Comput. Phys. Commun.* 174, 160–165.
- Nikezic, D., Yu, K.N., 2008. Analyses of light scattered from etched alpha-particle tracks in PADC. *Radiat. Meas.* 43, 1417–1422.
- Nikezic, D., et al., 2005. Application of the ray tracing method in studying α tracks in SSNTDs. *Radiat. Meas.* 40, 375–379.
- Oganesyan, V.R., et al., 2005. Investigation of the response of thin CR-39 polymer foils irradiated with light ions. *Nucl. Instr. Meth. B* 236, 289–294.
- Palmino, F., et al., 1999. Observation of nuclear track in organic material by atomic force microscopy in real time during etching. *Radiat. Meas.* 31, 209–212.
- Phillips, G.W., et al., 2006. Neutron spectrometry using CR-39 track etch detectors. *Radiat. Prot. Dosim.* 120, 457–460.
- Rana, M.A., et al., 2007. Characteristics of antiproton tracks in CR-39. *Radiat. Meas.* 42, 125–129.
- Sartowska, B., et al., 2005. Tracks of He and S ions with different energies in the PM-355 SSNTDs. Scanning electron microscopy investigations. *Radiat. Meas.* 40, 347–350.
- Séguin, F.H., et al., 2003. Spectrometry of charged particles from inertial-confinement-fusion plasmas. *Rev. Sci. Instrum.* 74, 975–995.
- Szydlowski, A., et al., 2005. Calibration of PM-355 nuclear track detectors; comparison of track diameter diagrams with track depth characteristics. *Radiat. Meas.* 40, 401–403.
- Yamauchi, T., et al., 2003. Track core size estimation in CR-39 track detector using atomic force microscope and UV-visible spectrophotometer. *Nucl. Instr. Meth. B* 208, 149–154.
- Yasuda, N., et al., 1999. Track sensitivity and the surface roughness measurements of CR-39 with atomic force microscope. *Radiat. Meas.* 31, 203–208.
- Yu, K.N., et al., 2007. Optical appearance of alpha particle tracks in CR-39 SSNTD. *Nucl. Instr. Meth. B* 263, 271–278.
- Zhai, K., et al., 2003. An atomic force microscopy investigation of the tracks made by C_1^+ – C_4^+ bombardment on CR-39 detectors. *Chin. Phys. Lett.* 20, 1947–1949.